Revised Manuscript 18-03116 for Annual Meeting Compendium of Papers

Investigation of Relationship between Train Speed and Bolted Rail Joint Fatigue Life Using Finite Element Analysis

Transportation Research Board 97th Annual Meeting

Submitted: November 8, 2017

[1]Hao Yin, Graduate Research Assistant
Phone: (217) 819-6305 / Email: haoyin2@illinois.edu

[2]Yu Qian, Ph.D., Assistant Professor
Phone: (803) 777-8184 / Email: yuqian@sc.edu

[1]J. Riley Edwards, P.E., Senior Lecturer and Research Scientist
Phone: (217) 244-7417 / Email: jedward2@illinois.edu

[3]Kaijun Zhu, Structure Engineer
Phone: (626) 304-2616 / Email: kzhu@saifulbouquet.com

[1]Rail Transportation and Engineering Center – RailTEC
Department of Civil and Environmental Engineering
University of Illinois at Urbana-Champaign
205 N. Mathews Ave., Urbana, IL 61801

[2] Department of Civil and Environmental Engineering
University of South Carolina
300 Main Street, Columbia, SC 29208

[3] Saiful Bouquet Structural Engineers Inc.
155 N Lake Ave. #600, Pasadena, CA 91101

4,093 Words, 2 Tables, 11 Figures = 7,343 Total Word Count

[2] Corresponding author

ABSTRACT

Reducing the allowable operating speed or placing temporary speed restrictions are common practices to prevent further damage to the track when defects are detected related to certain track components. However, the speeds chosen for restricted operation are typically based on past experience without considering the magnitude of the impact load around the rail joints. Due to the discontinuity of geometry and track stiffness at the bolted rail joints, an impact load always exists. Thus, slower speeds may not necessarily reduce the stresses at the critical locations around the rail joint area to a safe level. Previously, the relationship between speed and the impact load around the rail joints has not been thoroughly investigated. Recent research performed at the University of Illinois at Urbana-Champaign (UIUC) has focused on investigating the rail response to load at the joint area. A finite element model (FEM) with the capability of simulating a moving wheel load has been developed to better understand the stress propagation at the joint area under different loading scenarios and track structures. This study investigated the relationship between train speed and impact load and corresponding stress propagation around the rail joints to better understand the effectiveness of speed restrictions for bolted joint track. Preliminary results from this study indicated the contact force at the wheel-rail interface would not change monotonically with the changing train speed. In other words, when train speed was reduced, the maximum contact force at the wheel-rail interface may not necessarily reduce commensurately. Going forward, this method can be used to generate an optimized magnitude for speed reduction based on the specific loading environment and track structure with the objective of extending the track's service life and reducing the potential for component failures.

Keywords: Rail transit infrastructure, bolted rail joints, rail joint maintenance, finite element analysis, moving wheel loading, speed restriction, fatigue

INTRODUCTION

Two neighboring rails need to be connected to provide a uniform running surface for trains. Using rail joints or welding rails (i.e. continuous welded rail) are the two main methods of joining the rails together. With the increasing popularity of continuously welded rail (CWR) due to many maintenance and service life benefits, the number of in-service bolted joints has reduced significantly, and rail joint research has also decreased as a result. However, many bolted joints remain in the track, especially in the rail transit systems. Because of the unique loading environment in rail transit systems, such as high-frequency, high-repetition (i.e., number of load replications), defects associated with bolted rail joints still pose safety and operational challenges.

Rail end bolt-hole cracks and upper fillet cracks are two of the major challenges, which can cause a rail break or even loss of rail running surface. Previous research has concluded that the stress concentration around the rail end bolt-hole and the rail upper fillet areas are the primary reason for crack initiation and propagation (*1-3*). Without proper methods to identify the defects in the rail joints in a timely manner, the risk for damage to the track structure and/or derailments is higher (*4,5*).

To reduce the risk of accidents caused by potential failure of the track, temporary speed restrictions are typically applied to the sections where defects are detected. In October 2000, over 1,800 emergency speed restrictions were imposed and a nationwide track investigation and replacement program was conducted after Hatfield derailment in the United Kingdom (*6*). In February 2015, the Washington Metropolitan Area Transit Authority (WMATA) decided to slow down trains on some sections as a safety precaution to prevent incidents with rails that were potentially cracked or broken (*7*). Intuitively, to slow down trains would reduce the dynamic load on the rails and other track components. Due to the differences between track structures and operation practices, the speed restrictions among different freight railroads and transit agencies vary and are often based on past experience. Due to the discontinuity of geometry and track stiffness at the bolt rail joints, an impact load will always exist. Thus, slower operation speed may not necessarily reduce the stresses at the critical locations around the rail joint area to a safe level. Furthermore, the relationship between the rail stresses at the joint area and the operation speed has not been thoroughly investigated.

Recent research performed at the University of Illinois at Urbana–Champaign (UIUC) has focused on investigating the rail responses at the joint area. A finite element (FE) model has been developed to better understand the stress propagation at the joint area with different loading scenarios and track structures. This study investigated the relationship between train speed and the stresses around the rail end bolt-hole and upper fillet areas, which were identified as the most critical locations (*8*), with the objective of better understanding the effectiveness of speed restrictions. The predicted fatigue life of rail joints under different train speeds were also studied. Results indicate that the stresses in critical rail locations were not proportional to train speed, which does not align with conventional wisdom. In other words, lower train speeds do not necessarily ease the stress concertation around the joint area and consequently extend the fatigue life of rail joint.

OBJECTIVE AND SCOPE

The objective of this study is to investigate the relationship between the stress distributions and the consequent fatigue life at the critical locations around the rail joint area and train speed. Specifically, stresses at the rail-wheel contact interface, the rail end bolt-hole, and the rail end upper fillet will be investigated with the objective of evaluating the effectiveness of speed restrictions. A FE model that was previously developed to study optimal joint bar configurations (*8,9*) was adapted to simulate moving wheel loadings with various train speeds. The fatigue life of upper fillet area was also estimated with a fatigue life predictive model based on results from the FE analysis. Findings from this study can help to better understand the relationship between train speed and the fatigue life of rail joint and will aid in the refinement of future guidelines for speed restrictions to be more reflective of the stress state of the track and its components.

NUMERICAL SIMULATION APPROACH

A commercially available software known as *Abaqus/CAE* was selected to perform the FE simulations. A linear finite element model of rail joint system that was previously developed, calibrated, and validated was further refined to simulate the dynamic response of the rail joint system to the impact load caused by moving wheels. For the fatigue life analysis, the commercially available fatigue life analysis software *fe-safe* was selected to perform the prediction. The loading history of the moving wheel passing the gap of the rail joint obtained from the dynamic FE analysis was then used as the input for the fatigue life prediction, the estimated fatigue life (total cycle number of wheel passing before damage) was obtained as the results of the fatigue life analysis. The procedure of bolted rail joint FE analysis and fatigue life analysis is illustrated in **Figure 1**.

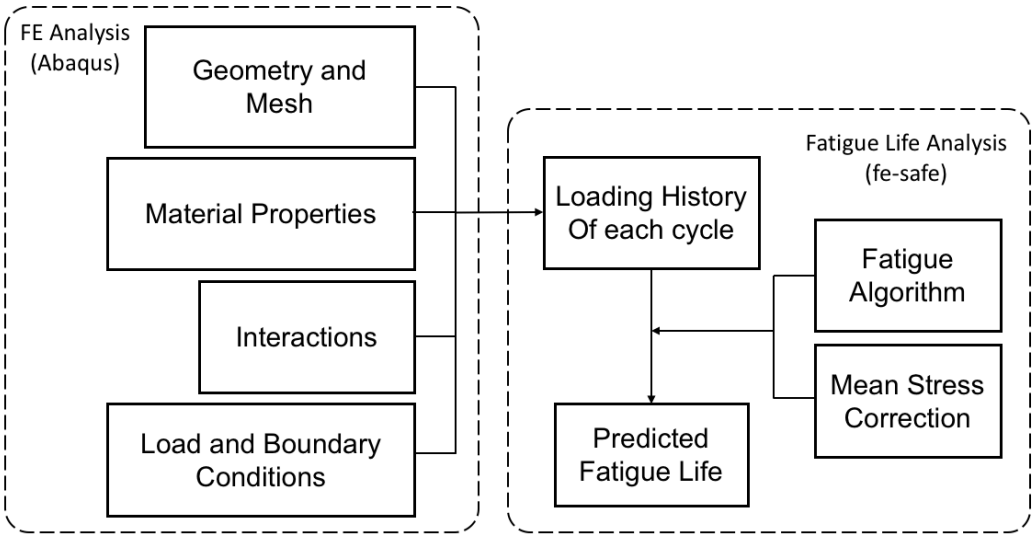

FIGURE 1 Procedure used for FE analysis of bolted rail joint and for fatigue life prediction

Dynamic FE Analysis Model

In order to gain insight into the response of the rail joint due to the impact loading caused by each wheel pass, a dynamic FE model was developed using Abaqus/CAE Explicit (**Figure 2)**.

The 115RE rail and standard joint bars were selected to represent a typical joint used in rail transit systems in the United States. The centermost crosstie spacing was 18 in. (45.7 cm), and other crossties were spaced at 22.5 in. (57.2 cm) on center. The total length of each rail was 216 in. (548.6 cm), based on the sensitivity analysis of rail length published in an earlier publication (*8*), the length of each rail modeled with 3-D deformable solid elements set to 36 in. (91.4 cm), and the remaining 180 in. (457.2 cm) of each rail was simplified by assigning rail section properties to linear beam elements. The gap (w) between sending rail and receiving rail was set to $w = 0.125$ in. (0.318 cm), and the initial height mismatch (h_{ini}) between the sending rail and receiving rail was also introduced in this dynamic FE model to better simulate the geometric imperfections at the rail joints caused by poor assembly, ground settlement, etc. Based on a similar study of the mechanical responses to the height mismatch at the rail joint (*10*), a height mismatch of $h_{ini} = 0.005$ in. (0.013 cm) was selected to obtain the rail response to the impact load when the wheel passing the gap. For the geometry of wheel, the diameter of wheel was set to $R = 17$ in. (43.2 cm), which was a typical size of railcar wheel used in heavy rail transit systems, such as the MTA New York City Transit Authority. Due to the fact that the behavior of rail joint system was primarily studied in the vertical plane and the models were loaded vertically and symmetrically in the

longitudinal direction of the rail, the railcar wheel was modeled as a cylinder without a flange. **Figure 3** shows the components of FE model generated in the simulation.

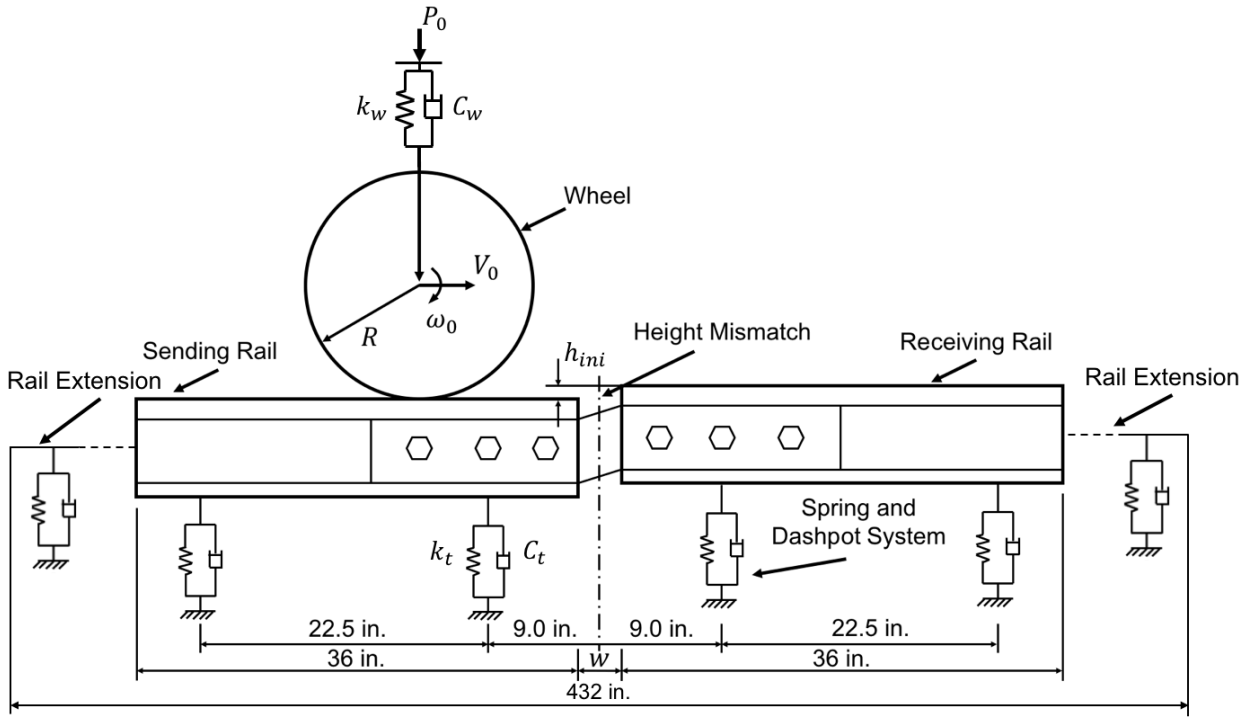

FIGURE 2 Schematic diagram of UIUC's FE model of bolted rail joint

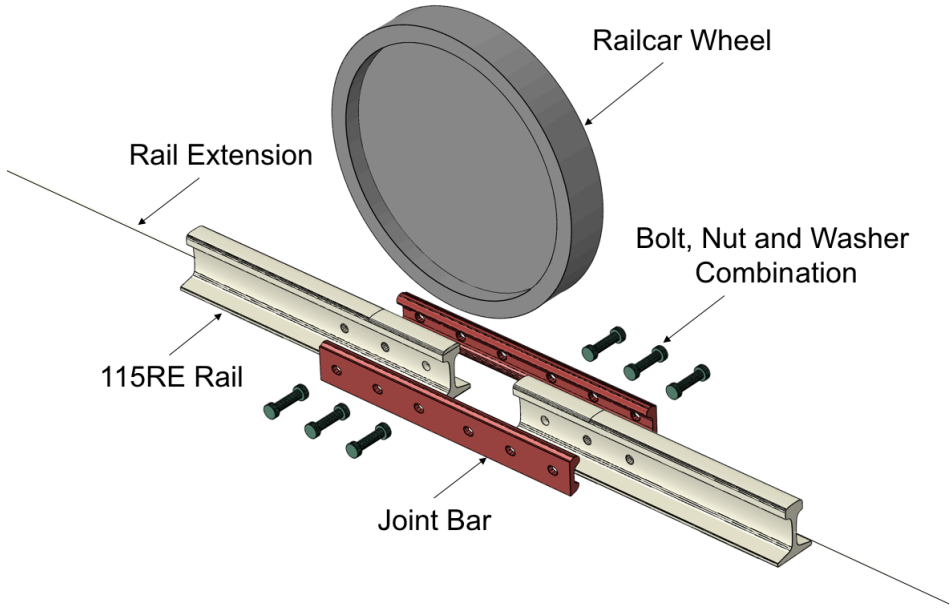

FIGURE 3 Components of the bolted rail joint assembly used in the dynamic FE model

Material Properties

All the parts (i.e. wheel, rail, rail joint) were assumed to behave elastically in the dynamic FE analysis and a correction of long-term behavior of materials was performed in conjunction with the fatigue life analysis. The Young's modulus, Poisson's ratio, and the density of the wheel, rails, rail joints, and bolts were assigned as 29,000 ksi (199.9 GPa), 0.33, and 0.283 lb/in^3 (7833.4 kg/m^3), respectively. The supporting system (e.g. crosstie, ballast, etc.) was represented in the model by linear spring and dashpot elements, with details of the simplifications included in an earlier publication (*8*). k_t and C_t were the spring stiffness and damper coefficients, and the equivalent springs and dampers were ones contributed from the crosstie, rail pad, ballast, subgrade, etc. Using a track modulus of 4,000 psi (27.58 MPa) provided by NYCTA and results from previous research pertaining to equivalent springs and dampers, $k_t = 90{,}000$ lbf/in. (15761 kN/m) and $C_t = 90$ lbf·s/in. (15.76 kN·s/m) were selected. Similarly, k_w and C_w were the spring stiffness and damper coefficient of springs representing the suspension system of a train car and $k_t = 1{,}000$ lbf/in. (175.13 kN/m) and $C_t = 0.8$ lbf·s/in. (0.14 kN·s/m) were selected, which are consistent with other studies (*10,11*).

Contact Interactions

Contact interactions between components were formulated using surface-to-surface contact discretization, and a master-slave surface pair was defined for each contact pair. This contact formulation method prevents large and undetected penetrations from nodes on the master surface into slave surface, providing more accurate stress and strain results compared with other methods (*12*). The basic Coulomb friction model with the penalty friction formulation was used to simulate the frictional force response at the contact interface. The maximum allowable frictional stress is related to contact pressure by the coefficient of friction (COF) between contacting bodies. The COFs of the contact pairs in the model were determined from literature and are summarized in **Table 1** (*13,14*).

TABLE 1 Coefficient of friction (COF) values used in the FE model

Frictional interaction	COF
Bolt-Rail interface	0.20
Bolt-Joint bar interface	0.20
Rail-Joint bar interface	0.20
Rail-Rail pad interface	0.30
Wheel-Rail interface	0.15

Load and Boundary Conditions

For loading conditions, since the stress distribution between the threaded bolt and nut is not the primary zone of interest in this study, the combination of the bolt, nut, and washer was simplified into a single component. The bolt torque moment was represented by bolt preload calculated with **Equation 1** by the bolt torque moment and bolt diameter *(15)*:

$$P_b = \frac{T}{KD} \tag{1}$$

where, P_b = bolt preload (lbf.)
T = bolt torque moment (lbf·in.)
K = coefficient of the bolt torque moment (43.8 – 56.2)
D = bolt diameter (in.)

The bolts used for the 115RE rail joints had a diameter D of 1 in. (2.54 cm), the torque moment T was chosen as 4,425 lbf·in. (500 N·m), and K = 45 was selected based on previous research (*8*). Thus, the bolt preload P_b was calculated as 22,000 lbf. (97.86 kN) per bolt. The axle load of 16,500 lbf. (73.40 kN) from train car was first applied on a spring element which represented the suspension, and then was vertically passed to the wheel. For boundary conditions, the displacements of each component at lateral and longitudinal direction of the rail were limited since the behavior of rail joint system was primarily studied in the vertical direction.

In addition, because the explicit solver was used for the dynamic FE analysis, the time increment size must be limited to a very small number to avoid numerical stability and convergence issues, and after a sensitivity study of the time increment size was conducted 0.0001s/step was selected. All of the constants and variables that were considered in the dynamic FE model are summarized in **Table 2**.

TABLE 2 Constants and variables for FE Model

Constants	
Crosstie Spacing (Center)	18 in. (45.7 cm)
Crosstie Spacing	22.5 in. (57.2 cm)
Rail Section	115RE Rail
Rail Length	216 in. (548.6 cm) - 36 in. (91.4 cm) with 3D elements 180 in. (457.2 cm) with 1D elements
Gap Height Mismatch, h_{ini}	0.005 in. (0.013 cm)
Gap Width, w	0.125 in. (0.318 cm)
Joint Bar Design	Standard Joint Bar
Bolt Preloading	22,000 lbf. (97.86 kN) per bolt
Wheel Radius	17 in. (43.2 cm)
Wheel Load	16,500 lbf. (73.40 kN)
Suspension Spring Stiffness	1,000 lbf/in. (175.13 kN/m)
Track Modulus Equivalent Spring Stiffness	4,000 psi (27.58 MPa) 90,000 lbf/in. (15761 kN/m)
Time Increment Size	0.0001s/step

Variables	
Train Speed (Wheel rolling speed, no slippage)	5 mph (8.0 km/h)
	10 mph (16.1 km/h)
	20 mph (32.1 km/h)
	30 mph (48.3 km/h)
	40 mph (64.4 km/h)
	50 mph (80.5 km/h)
	60 mph (96.6 km/h)

Fatigue Life Analysis

The fatigue life analysis was performed primarily based on the load history and stresses distribution calculated from the dynamic FE models. In addition to the FE analysis results, information of material properties, as well as the selection of the methods of fatigue algorithm and mean stress correction, were of great importance during the fatigue analysis. *fe-safe* was selected to perform the fatigue analysis for bolted rail joints taking into consideration the effects of various impact loads caused by various wheel speeds. The methodology used in this study is illustrated in **Figure 4**.

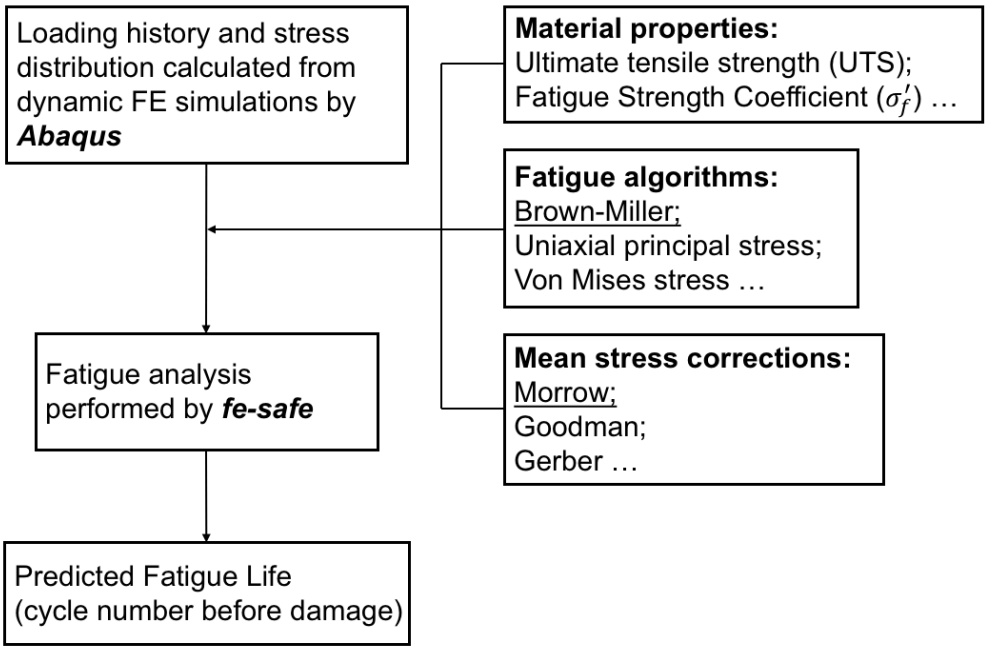

FIGURE 4 Fatigue life analysis methodology

Loading History

The wheel-rail contact force history obtained from the dynamic FE analysis was used as the load history for each cycle of wheel passing and was input directly into *fe-safe*. This load history was utilized as the base load, and was factored using a load factor function. The estimated fatigue life could be considered as the total cycles of loading that the system has experienced before damage occurs, namely, the total number of wheels passing over the rail joint before damage initiates.

Material Properties of Fatigue Life Analysis

Based on a test report provided by NYCTA, the ultimate tensile strength (UTS) of the steel used for 115RE rail was approximately 177.0 ksi (1220 MPa), strength at 10^7 cycles (Fatigue Limit) was 61.5 ksi (424 MPa), which were two key parameters used for the fatigue life analysis. The fatigue limit represents a cyclic stress amplitude below which the material does not fail and could be cycled indefinitely (i.e. an infinite fatigue life). For ductile steel specifically, the fatigue limit is the strength of the material at 10^7 cycles of loading. In other words, if the steel structural system could experience at least 10^7 cycles of loading without cracking or other damage, it is assumed that no fatigue damage would occur under the same loading conditions (*16*).

Fatigue Analysis Algorithms

The Brown-Miller criterion was selected for this specific fatigue analysis, which gave the most realistic fatigue life estimates for ductile metals. The Brown-Miller equation suggests that the maximum fatigue damage occurs on the plane which experiences the maximum shear strain amplitude, and that damage is a function of both this shear strain amplitude ($\Delta\gamma_{max}/2$) and the normal strain amplitude ($\Delta\varepsilon_n/2$). Accordingly, different from the conventional strain-life equation (**Equation 2**), the Brown-Miller equation (**Equation 3**) alters the left-hand side of the equation with the addition of shear strain amplitude and normal strain amplitude (*17*).

$$\frac{\Delta\varepsilon}{2} = \frac{\sigma_f'}{E}\left(2N_f\right)^b + \varepsilon_f'\left(2N_f\right)^c \quad (2)$$

where, $\Delta\varepsilon/2$ = applied strain amplitude
$2N_f$ = endurance in reversals
σ_f' = fatigue strength coefficient
ε_f' = fatigue ductility coefficient
b = fatigue strength exponent
c = fatigue ductility exponent

$$\frac{\Delta\gamma_{max}}{2} + \frac{\Delta\varepsilon_n}{2} = C_1\frac{\sigma_f'}{E}\left(2N_f\right)^b + C_2\varepsilon_f'\left(2N_f\right)^c \quad (3)$$

Where, $\Delta\gamma_{max}/2$ = shear strain amplitude
$\Delta\varepsilon_n/2$ = normal strain amplitude
C_1 = 1.65 (constant)
C_2 = 1.75 (constant)

The constants $C_1 = 1.65$ and $C_2 = 1.75$ were derived based on the assumption that cracks initiate on the plane of maximum shear strain. However, for complex variable amplitude loading, it was found that better agreement with test results was obtained by assuming that the most damaged plane was the one that produced the highest value of $(\Delta\gamma_{max}/2 + \Delta\varepsilon_n/2)$. For that case, constants C_1 and C_2 will have slightly different values on this plane. Nevertheless, the values shown in **Equation 3** could be applied generally (*18*).

Mean Stress Corrections

Typically, it is common for a load history to have a non-zero mean stress, σ_m, which is defined in **Equation 4**. The fatigue performance would vary as the mean stress changes. The influence of mean stress can be characterized as the influence of stress amplitude, σ_a, the distance of minimum stress to maximum stress in a fatigue loading cycle (**Equation 5**).

$$\sigma_m = \frac{\sigma_{max} + \sigma_{min}}{2} \quad (4)$$

$$\sigma_a = \frac{\sigma_{max} - \sigma_{min}}{2} \quad (5)$$

where, σ_m = mean stress (psi)
σ_a = stress amplitude (psi)
σ_{max} = maximum stress (psi)
σ_{min} = minimum stress (psi)

Generally, it can be observed that for mean stress, a tensile mean stress has a detrimental effect on endurance cycles N_f, whereas a compressive mean stress has a beneficial effect. For stress amplitude, the endurance cycles N_f increases as the applied stress amplitude σ_a decreases (*19*). To correct the influence of mean stress, the Morrow mean stress correction was adopted for Brown-Miller criterion. After the application of Morrow mean stress correction, the Brown-Miller equation (**Equation 3**) becomes **Equation 6**, with a corrected elastic term by subtracting the mean normal stress on the plane, $\sigma_{n,m}$ (*20*).

$$\frac{\Delta\gamma_{max}}{2} + \frac{\Delta\varepsilon_n}{2} = C_1 \frac{\left(\sigma_f' - \sigma_{n,m}\right)}{E}\left(2N_f\right)^b + C_2\varepsilon_f'\left(2N_f\right)^c \quad (6)$$

where, $\sigma_{n,m}$ = mean normal stress (psi)

DISCUSSION OF THE RESULTS

Critical outputs from the dynamic FE model, such as the wheel-rail contact force, Von Mises stress around rail end bolt-hole, Von Mises stress at rail-end upper fillet, and the vertical displacement at rail-end, were analyzed. **Figure 5** shows examples of aforementioned parameters when the wheel was passing different locations around the joint calculated in the simulation at train speed of 20 mph (32.1km/h).

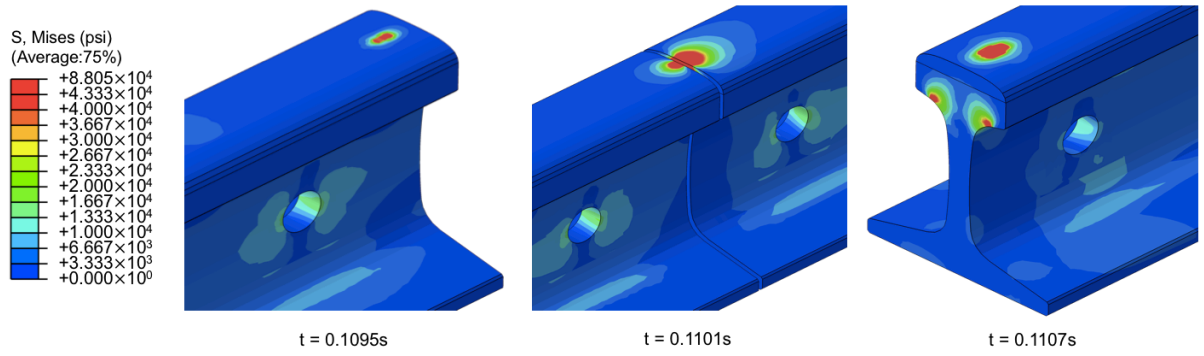

(a)

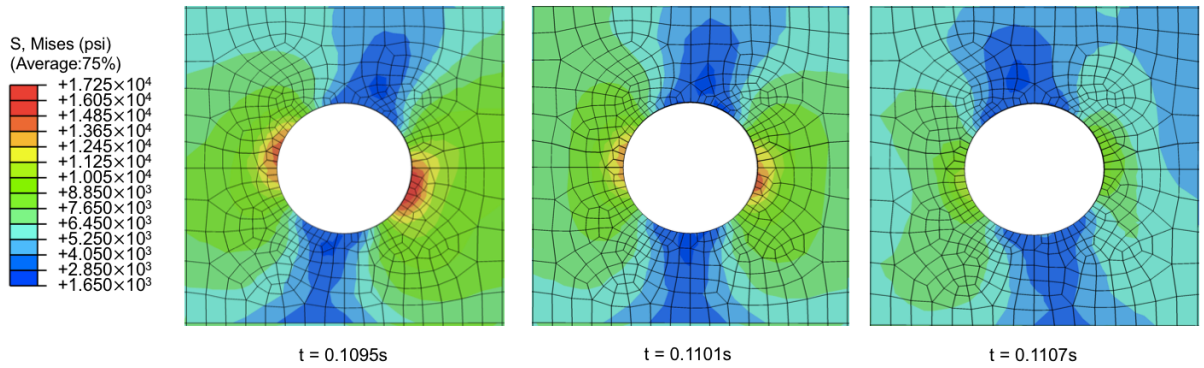

(b)

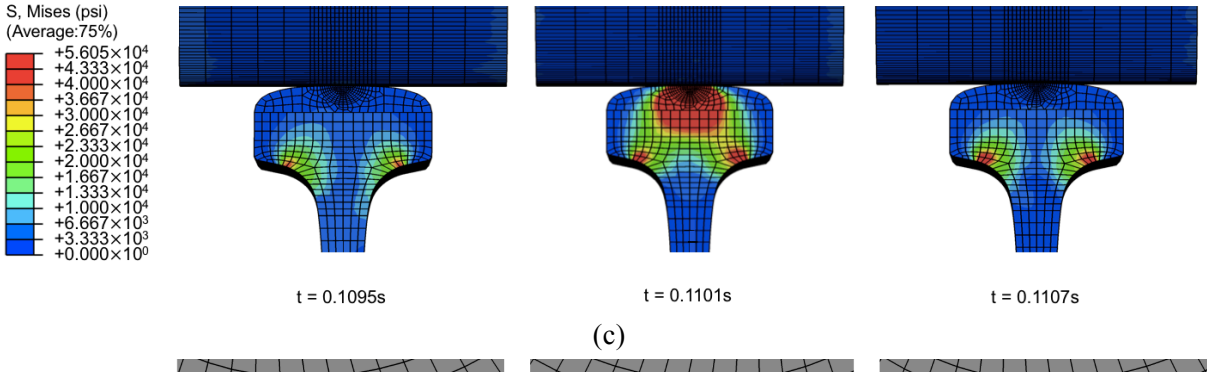

(c)

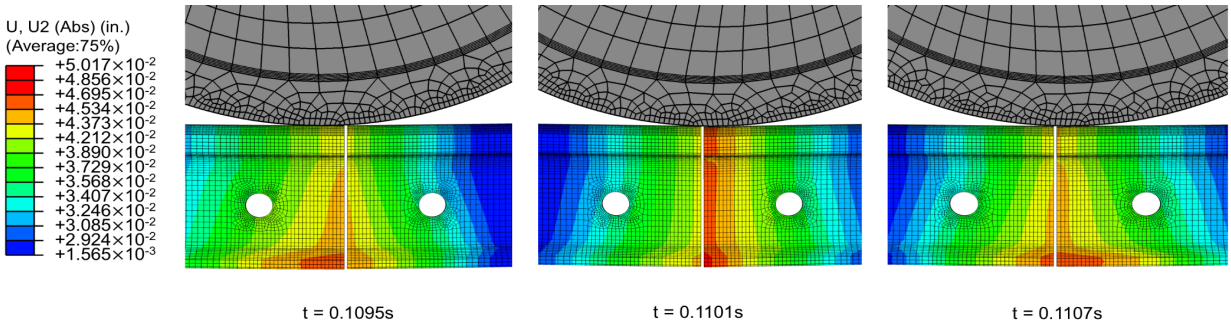

(d)

FIGURE 5 Examples of the simulation results at train speed of 20 mph (32.1km/h): (a) wheel-rail contact patch (b) Von Mises stress around rail-end bolt hole (c) Von Mises stress at rail-end upper fillet (d) vertical displacement at rail-end

The loading history of the vertical contact force at the wheel-rail interface when the wheel was moving at a speed of 20 mph (32.1 km/h) is shown in **Figure 6**. It should be noticed that the original data from the simulation was the time history of wheel-rail contact force, and it was modified by changing the independent variable (x-axis) from the time to the relative wheel position on the rail surface. As such, the starting point was set to the left end of the joint bar and the ending point was set to the right end of joint bar as shown in the schematic drawings at the bottom of **Figure 6**. When the wheel was running on the sending rail approaching to the gap, the wheel-rail contact force was relatively stable, around 16,500 lbf. (73.4 kN), approximately the same value as the applied wheel load, with certain variation due to the wheel and track vibration. When the wheel rolled over the gap between the two rails, an unloading stage was observed. Once the wheel contacted with the second rail after passing the gap, a peak contact force (P1) of 40,832 lbf. (181.6 kN), was recorded which was the response of the rail to the impact of the moving wheel. Another peak contact force (P2) showed up after P1, which was the response of the track system.

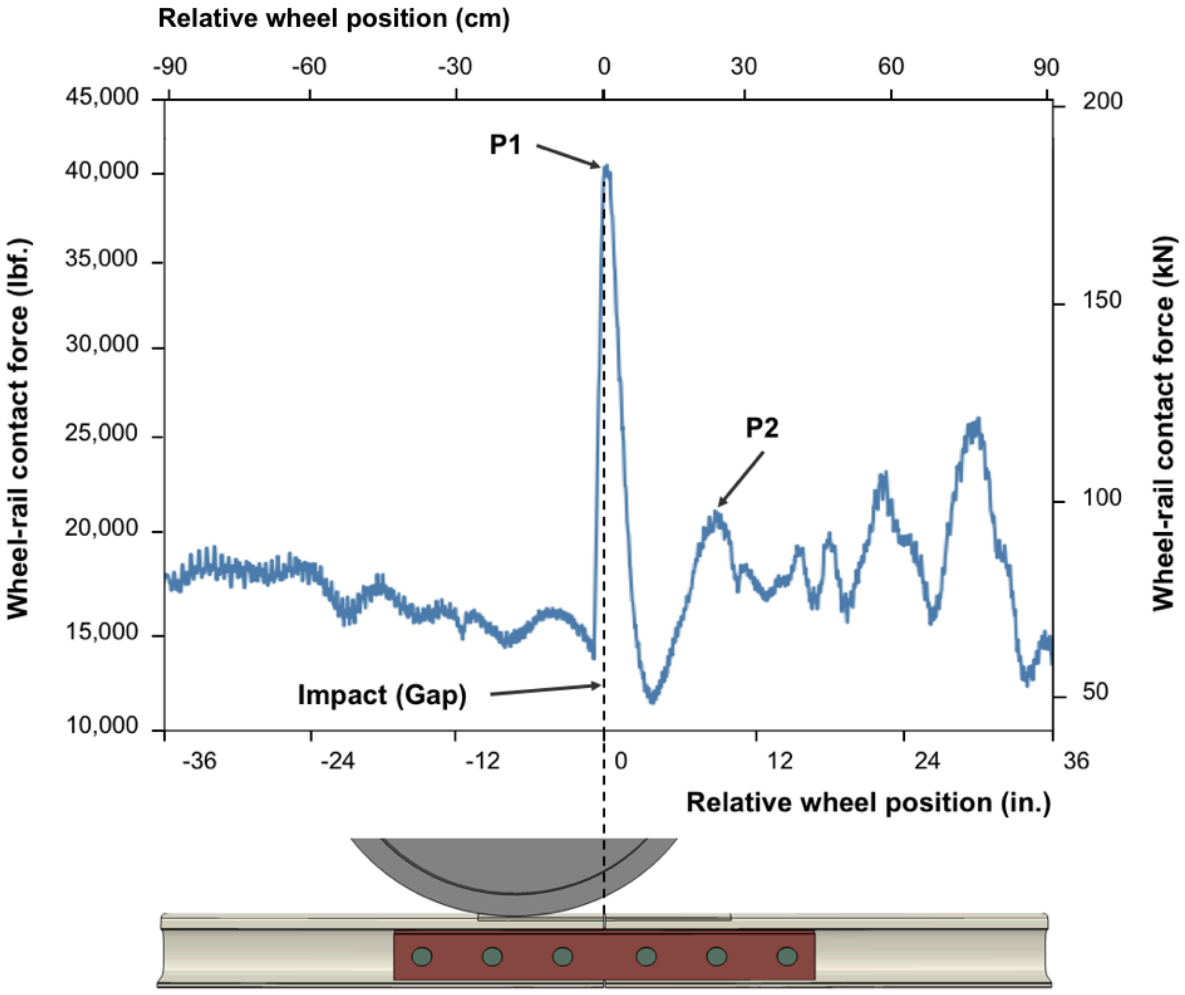

FIGURE 6 Contact force history of wheel-rail interface of Bolted Rail Joint at train speed of 20 mph (32.1km/h)

Figure 7 shows the mechanical response of rail to the impact load due to the wheel rolling over the gap at various train speeds. **Figure 7(a)** plots all the peak wheel-rail contact force (P1) values for the different simulations that having different train speeds. Note the first peak contact force, P1, is always higher than the second peak contact force, P2(*21*). By comparing the P1 values at different operation speeds, it is clear that the magnitude of P1 was not related to train speed in a linear manner. In other words, reducing train speed from 60 mph (96.6 km/h) to 5 mph (8.0 km/h), the peak wheel-rail contact force did not reduce monotonically. When the operation speed was 60 mph (96.6 km/h), the value of P1 was 40,253 lbf. (179.1kN), when the operation speed reduced to 50 mph (80.5 km/h) and 40 mph (64.4 km/h), P1 reduced to 37,800 lbf. (168.1 kN) and 36,500 lbf. (162.4 kN), respectively. However, when the operation speed further reduced to 30 mph (48.3 km/h) and 20 mph (32.1 km/h), P1 increased to 41,916 lbf. (186.5 kN) and 40,832 lbf. (181.6 kN), respectively. This finding was counterintuitive, and the same trend was also observed for the maximum Von Mises stress around the bolt-hole and upper fillet area in **Figure 7(b)(c).**

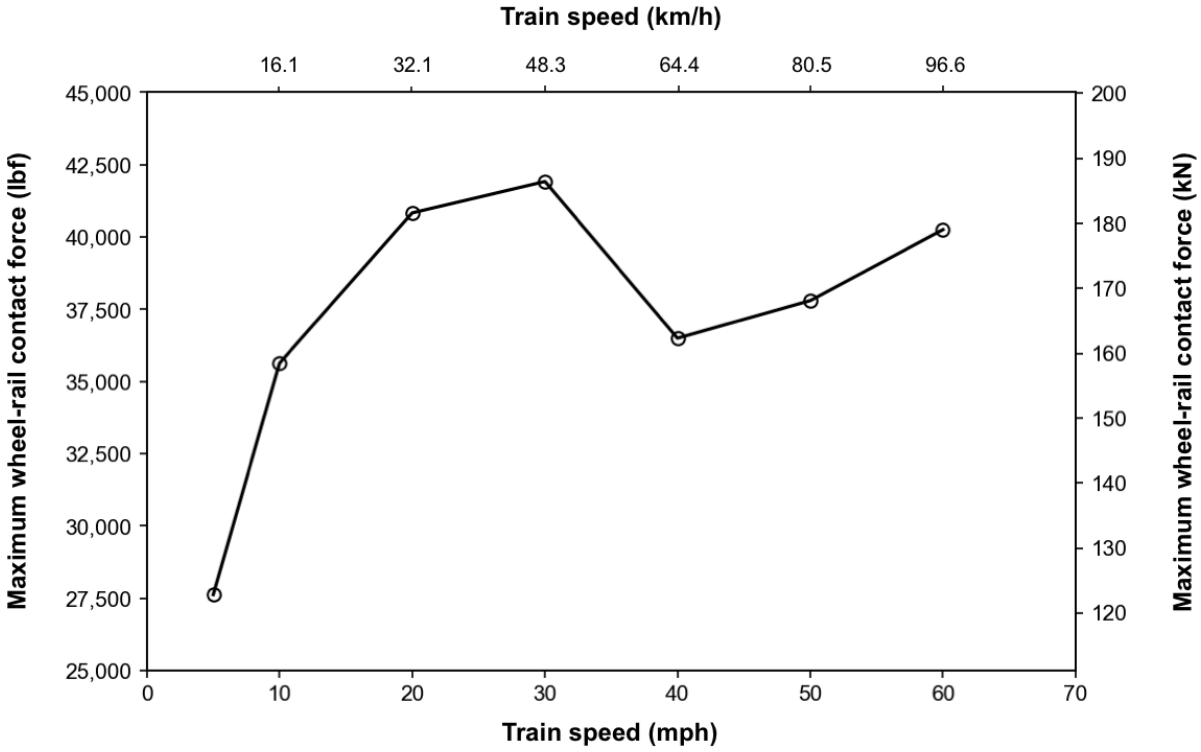

(a)

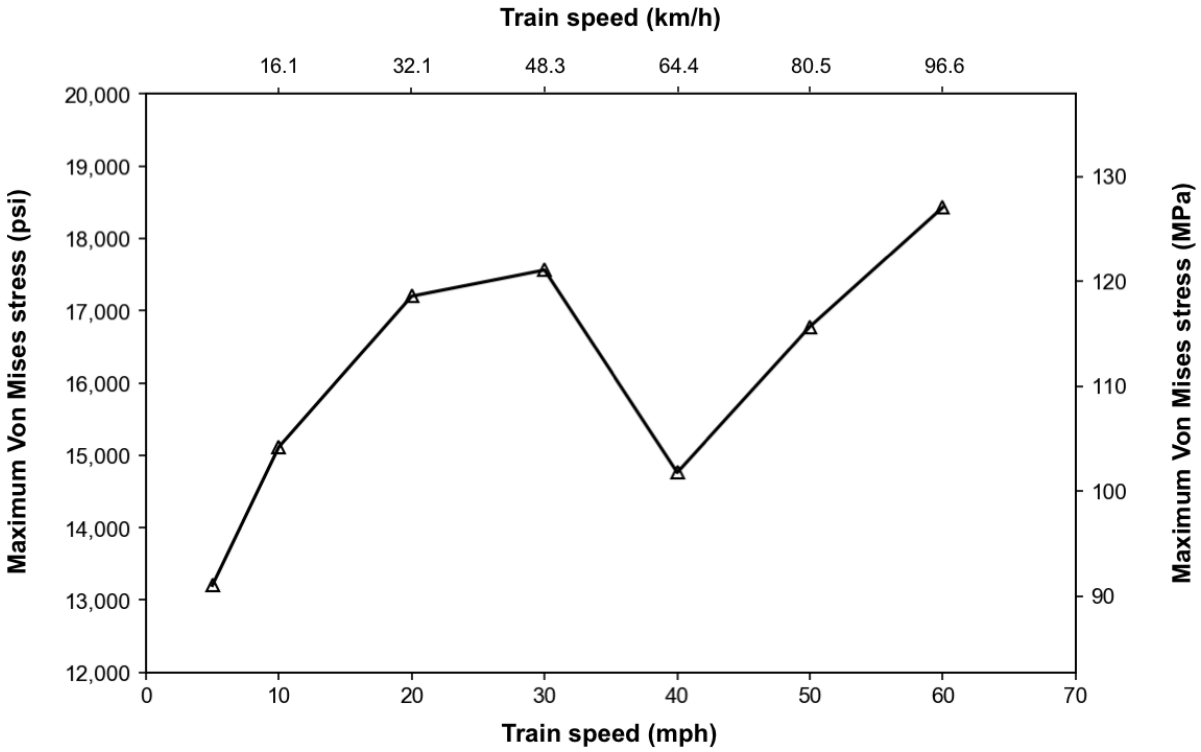

(b)

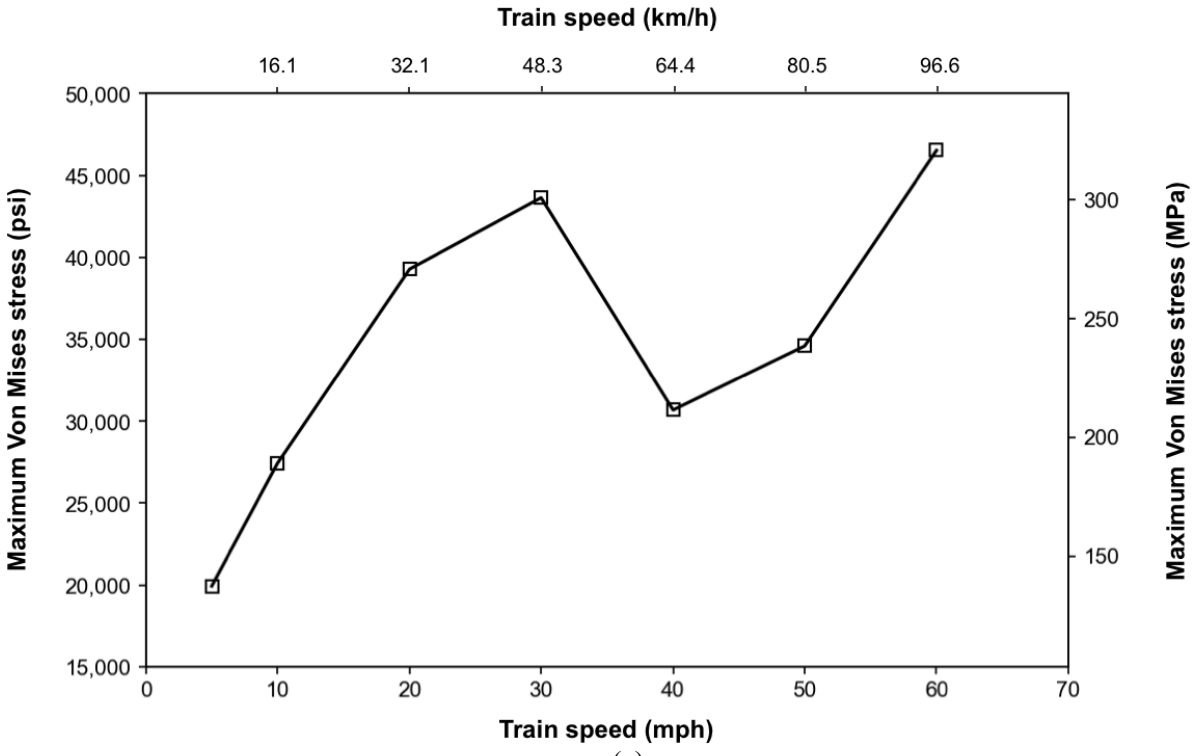

(c)

FIGURE 7 Mechanical responses of rail joint at various operation speeds: (a) Maximum contact force at the wheel-rail interface (b) Maximum Von Mises stress around the rail-end bolt hole (c) Maximum Von Mises stress at rail-end upper fillet

Prevailing rail industry knowledge would state that the contact force generally decreases monotonically decreasing train speed (*21*), but findings shown in **Figure 7** from this study are not in agreement with the literature. The concept that dynamic load increases with the traveling speed increases in the literature is based on the well-established vehicle-track interaction theory without considering the joints. However, there are two important differences between this study and existing literature: 1) the gap between the two rails and 2) the differential displacement of the two rails at the joint. Due to the gap between the two rails, the sending rail and the receiving rail will not have the same displacement at the same time. When the wheel is approaching the end of the sending rail, the displacement of the end of the sending rail increases. The displacement of the sending rail will cause the joint bar to move together. The displacement of the joint bar will then cause the displacement of the receiving rail. The sending rail will reach its maximum displacement when the wheel is on top of the end of the rail (*8*), right before the wheel rolls over the gap. However, the receiving rail will not reach the same displacement simultaneously. The differential displacement of the two rails will cause additional height mismatch (h_w) before the wheel hit the receiving rail (shown in **Figure 8**). Previous research has shown the maximum contact force when the wheel hits the receiving rail increases as a function of height mismatch *(10)*. **Figure 9** shows the height mismatch increased when the speed decreased. **Figure 8** and **Figure 9**, when combined, show that when the operation speed reduced, the rail height mismatch would increase, and as a result, the maximum contact force could increase. Due to the rail height mismatch at the joint and the relationship of the operation speed and the rail mismatch discussed above, the maximum contact force may not decrease monotonically with the operation speed decreases, as illustrated again in **Figure 10**.

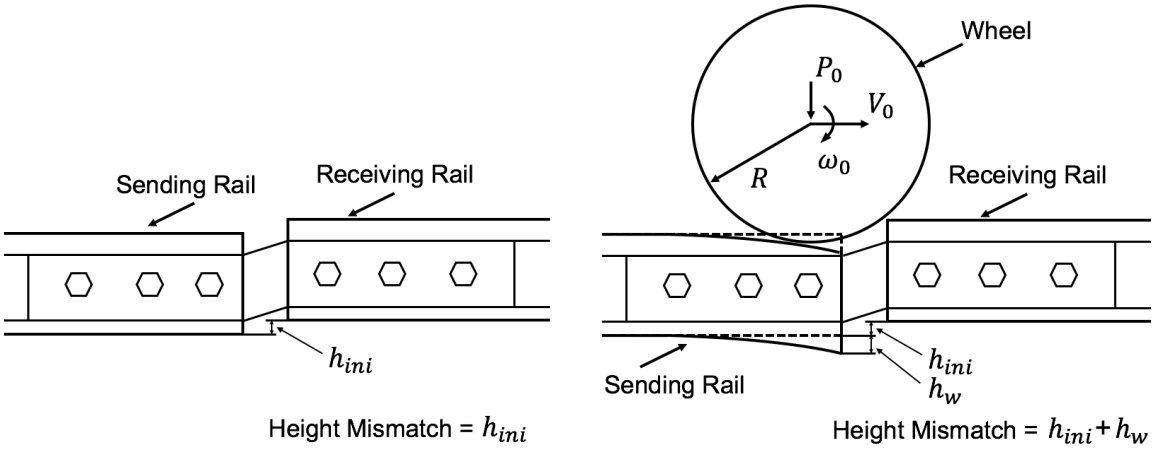

(a) Height mismatch before wheel loading (b) Height mismatch under wheel loading

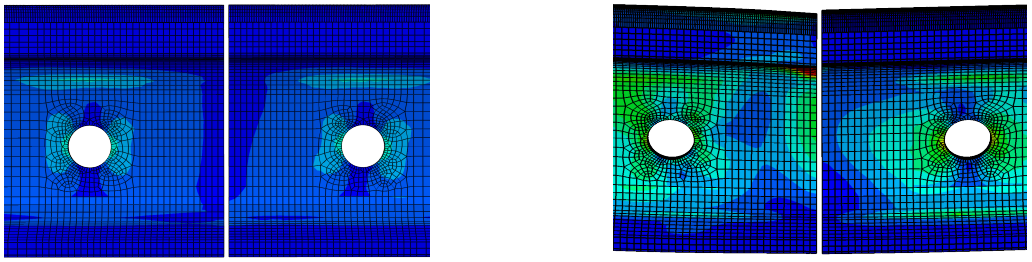

(c) Height mismatch before wheel loading in FEM (d) Height mismatch under wheel loading in FEM

FIGURE 8 Schematic drawings and FEM examples of height mismatch caused by wheel

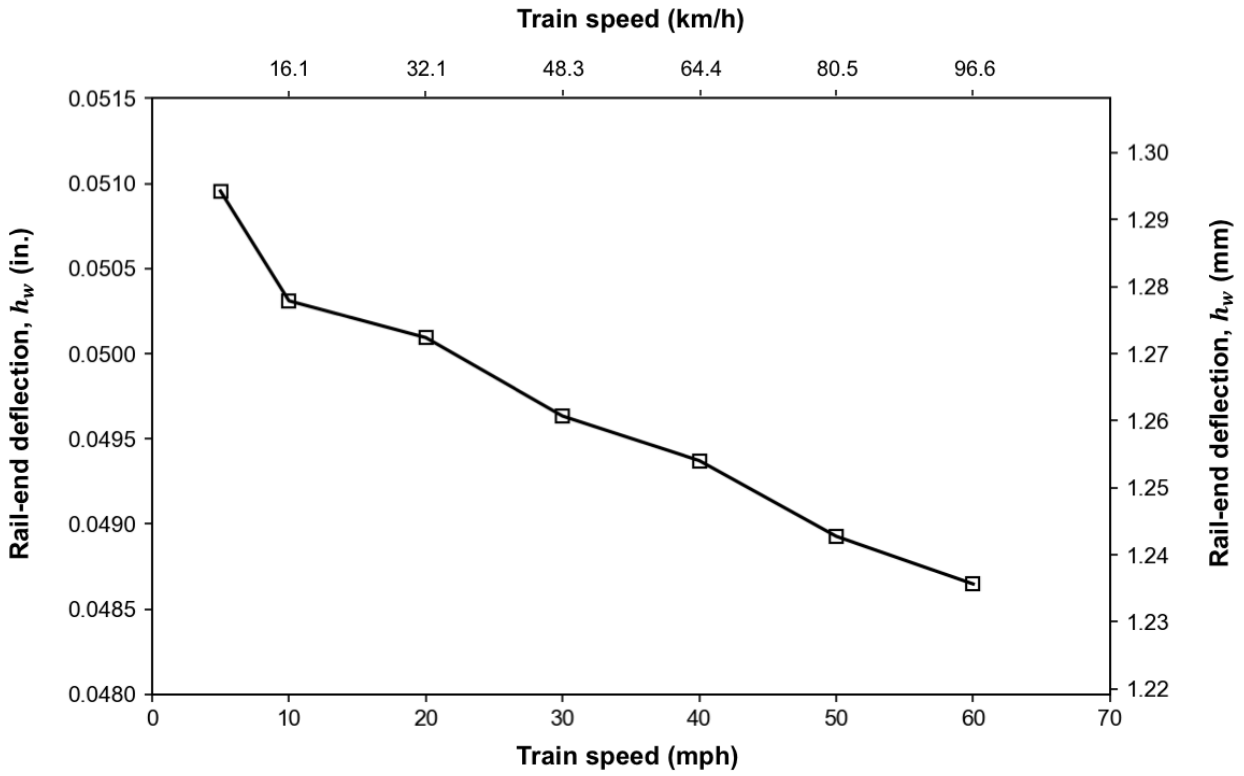

FIGURE 9 Rail height mismatch caused by wheel loading at various operation speeds, h_w

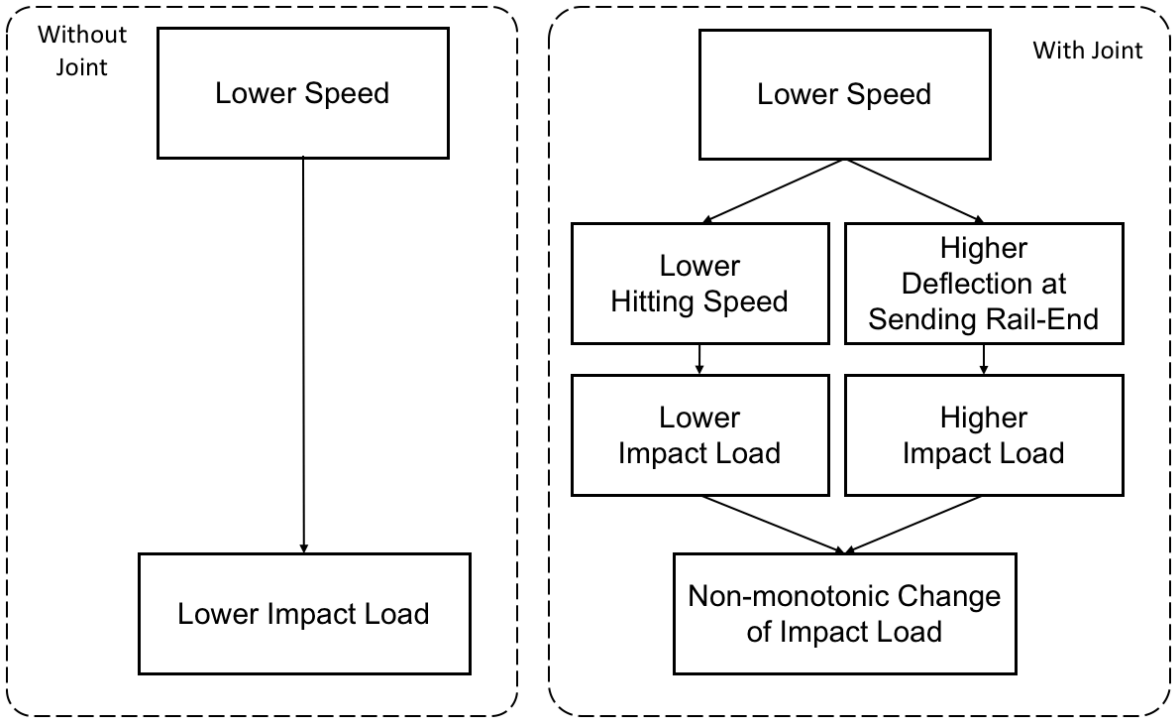

FIGURE 10 Relationship between operation speed and contact force

Based on the results shown in **Figure 7(b)(c),** the stresses calculated around the bolt hole area were significantly smaller than the stresses around the upper fillet area, which was also shown in a previous study (*8*, 9). Based on this result, the rail-end upper fillet area was selected to perform the fatigue life analysis. **Figure 11** presents the fatigue life of the upper fillet predicted based on the loading history (see **Figure 6** for example) with the same configurations but different train speeds simulated in this study. Assume trains continue to operate at a speed of 60 mph (96.6 km/h), the estimated fatigue life would be 6.6×10^5 wheel passes. If a speed restriction was issued, and the speed reduced to 40 mph (64.4 km/h) or 10 mph (16.1 km/h), the estimated fatigue life would increase to 4.2×10^6 or 2.9×10^6 wheel passes, an increase of 536% and 339%, respectively. However, if the speed was reduced to 30 mph (48.3 km/h) or 20 mph (32.1 km/h), the estimated fatigue life would decrease to 4.3×10^5 or 1.7×10^5 wheel passes, a reduction of 74% and 35%, respectively. Also, the trend line of estimated fatigue life shows that the fatigue life at rail-end upper fillet was highly correlated with mechanical responses of rail (shown in **Figure 7**), and the estimated fatigue life was negatively correlated with the impact load applied to the rail joint (i.e. maximum wheel-rail contact force).

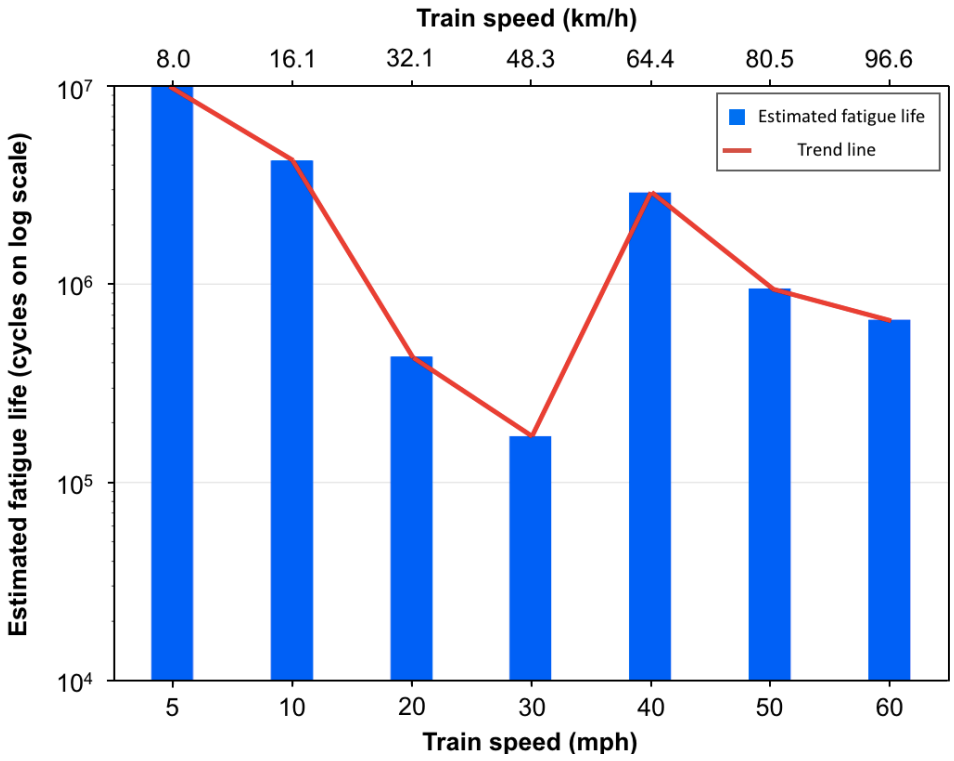

FIGURE 11 Estimated fatigue life at rail-end upper fillet at various operation speeds

CONCLUSIONS

This paper presents results from detailed FE simulations of the contact force at the wheel-rail interface, the stress distribution around the rail end bolt-hole, and rail end upper fillet areas under moving wheel loadings. Seven different train speeds, varying from 5 mph to 60 mph, were simulated and compared to investigate the relationship between the fatigue life and train speed. The following conclusions can be drawn from the results of this study:

1. At a rail joint, the contact force at the wheel-rail interface does not change monotonically with the

changing train speed. When train speed was reduced, the maximum contact force at the wheel-rail interface may not necessarily reduce.
2. The non-monotonic relationship between the contact force at the wheel-rail interface and train speed was due to both the negative correlation of the rail height mismatch and the operation speed and the positive correlation of the dynamic load and the operation speed.
3. When placing a temporary speed restriction, reducing train speed may not necessarily extend the fatigue life of the track with joints. If reducing the operation speed improperly, the fatigue life of the rail joints could be reduced.

ACKNOWLEDGEMENTS

This research was partially funded by WSP, under contract with New York City Transit Authority (NYCTA). The opinions expressed in this article are solely those of the authors and do not represent the opinions of the funding agency. Additional supporting funding was provided by National University Rail (NURail) Center, a USDOT-OST Tier 1 University Transportation Center. J. Riley Edwards has been supported in part by grants to the UIUC Rail Transportation and Engineering Center (RailTEC) from CN and Hanson Professional Services.

REFERENCES

1. Mayville, R. A. and R. G. Stringfellow. 1993. *Development and Application of Rail Defect Fracture Models to Assess Remedial Actions*. Final Report, DOT/FRA/ORD-93/33.
2. Mayville, R. A. and R. G. Stringfellow. 1995. Numerical Analysis of a Railroad Bolt Hole Fracture Problem. *Theoretical and Applied Fracture Mechanics*, Volume 24, Issue 1, pp. 1-12.
3. Carolan, M.E., D.Y. Jeong, and A.B. Perlman. 2014. Engiheering Studies on Joint Bar Integrity , Part II: Finite Element Analysis. Proceedings of the 2014 Joint Rail Conference, JRC 2014-3708, April 2014, Colorado Springs, CO.
4. National Transportation Safety Board Railroad Accident Brief 1409: *Derailment and Subsequent Collision of Two Metro-North Passenger Trains*.
5. Schlesinger, D. 2016. *Sources of Transportation Accident Information*. Proceedings of the 2016 Joint Rail Conference, JRC 2016-5836, April 2016, Columbia, SC.
6. Smith, R.A., 2003. The wheel–rail interface—some recent accidents. *Fatigue & Fracture of Engineering Materials & Structures, 26*(10), pp.901-907.
7. Lazo, Luz, 2015. Metro speed restrictions could add to commuters' travel time. *The Washington Post, 3 February 2015*.
8. Zhu, K., J. R. Edwards, Y. Qian, and B. Andrawes. 2016. Finite Element Analysis of the Effects of Bolt Condition on Bolted Rail Joints Stresses. *Transportation Research Record: Journal of the Transportation Research Board*, Transportation Research Board of the National Academies, No. 2545, pp. 36-45.
9. Zhu, K., Y. Qian, J. R. Edwards, and B. Andrawes. 2017. Finite Element Analysis of Rail End Bolt-Hole and Fillet Stress on Bolted Rail Joints. *Transportation Research Record: Journal of the Transportation Research Board*, Transportation Research Board of the National Academies, No. 2607, pp. 33-42.
10. Soylemez, E. and Ciloglu, K., 2016. Influence of track variables and product design on insulated rail joints. *Transportation Research Record: Journal of the Transportation Research Board*, (2545), pp.1-10.
11. Uzzal, R.U.A., Ahmed, W. and Rakheja, S., 2008. Dynamic analysis of railway vehicle-track interactions due to wheel flat with a pitch-plane vehicle model. *Journal of Mechanical Engineering*, 39(2), pp.86-94.

12. Zhang, Z., Wei, S., Andrawes, B., Kuchma, D.A. and Edwards, J.R., 2016. Numerical and experimental study on dynamic behaviour of concrete sleeper track caused by wheel flat. *International Journal of Rail Transportation,* 4(1), pp.1-19.
13. Yamaguchi, Y., 1990. *Tribology of plastic materials: their characteristics and applications to sliding components* (Vol. 16). Elsevier.
14. Kernes, R.G., Edwards, J.R., Dersch, M.S., Lange, D.A. and Barkan, C.P., 2011, January. Investigation of the dynamic frictional properties of a concrete crosstie rail seat and pad and its effect on rail seat deterioration (RSD). *In Transportation Research Board 91st Annual Meeting.*
15. Wen, Z., Jin, X. and Zhang, W., 2005. Contact-impact stress analysis of rail joint region using the dynamic finite element method. *Wear*, 258(7), pp.1301-1309.
16. Matake, T., 1977. An explanation on fatigue limit under combined stress. *Bulletin of JSME*, 20(141), pp.257-263.
17. Brown, M.W. and Miller, K.J., 1973. A theory for fatigue failure under multiaxial stress-strain conditions. *Proceedings of the Institution of Mechanical Engineers*, 187(1), pp.745-755.
18. Zheng, Z.G., Sun, T., Xu, X.Y., Pan, S.Q. and Yuan, S., 2014. Numerical simulation of steel wheel dynamic cornering fatigue test. *Engineering Failure Analysis*, 39, pp.124-134.
19. Glinka, G., Wang, G. and Plumtree, A., 1995. Mean stress effects in multiaxial fatigue. *Fatigue & fracture of engineering materials & structures*, 18(7–8), pp.755-764.
20. Morrow, J., 1968. Fatigue design handbook. *Advances in engineering*, 4(3.2), pp.21-29.
21. Zhai, W.M., 2007. Vehicle-track coupling dynamics. *China Railway Press, Beijing, People's Republic of China*.